Ahmad, Saeed; Liao, Yongping; Hussain, Aqeel; Zhang, Qiang; Ding, Er-Xiong; Jiang, Hua; Kauppinen, Esko I.

Systematic investigation of the catalyst composition effects on single-walled carbon nanotubes synthesis in floating-catalyst CVD

Published in:
Carbon

DOI:
10.1016/j.carbon.2019.04.026

Published: 01/08/2019

Document Version
Peer-reviewed accepted author manuscript, also known as Final accepted manuscript or Post-print

Please cite the original version:
Ahmad, S., Liao, Y., Hussain, A., Zhang, Q., Ding, E.-X., Jiang, H., & Kauppinen, E. I. (2019). Systematic investigation of the catalyst composition effects on single-walled carbon nanotubes synthesis in floating-catalyst CVD. *Carbon*, *149*, 318-327. https://doi.org/10.1016/j.carbon.2019.04.026

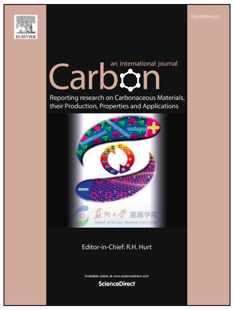

Systematic investigation of the catalyst composition effects on single-walled carbon nanotubes synthesis in floating-catalyst CVD

Saeed Ahmad, Yongping Liao, Aqeel Hussain, Qiang Zhang, Er-Xiong Ding, Hua Jiang, Esko I. Kauppinen

PII: S0008-6223(19)30353-7

DOI: https://doi.org/10.1016/j.carbon.2019.04.026

Reference: CARBON 14110

To appear in: *Carbon*

Received Date: 14 February 2019

Revised Date: 31 March 2019

Accepted Date: 7 April 2019

Please cite this article as: S. Ahmad, Y. Liao, A. Hussain, Q. Zhang, E.-X. Ding, H. Jiang, E.I. Kauppinen, Systematic investigation of the catalyst composition effects on single-walled carbon nanotubes synthesis in floating-catalyst CVD, *Carbon* (2019), doi: https://doi.org/10.1016/j.carbon.2019.04.026.

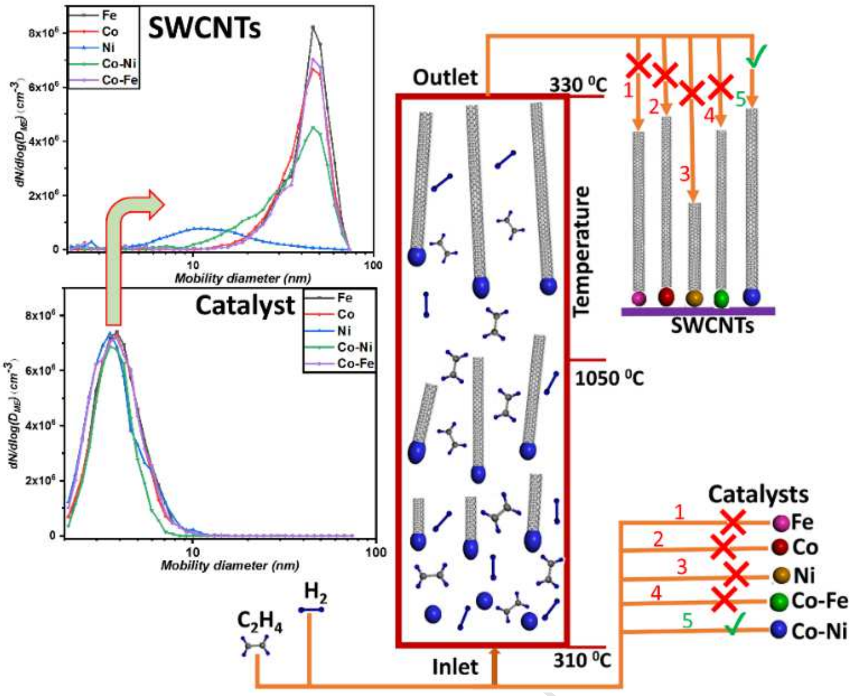

Graphical abstract

Systematic investigation of the catalyst composition effects on single-walled carbon nanotubes synthesis in floating-catalyst CVD

Saeed Ahmad, Yongping Liao, Aqeel Hussain, Qiang Zhang*, Er-Xiong Ding, Hua Jiang and Esko I. Kauppinen*

Department of Applied Physics, Aalto University School of Science, P.O. Box 15100, FI-00076 Aalto, Finland.

Abstract

Enormous technological promise of single-walled carbon nanotubes (SWCNTs) can only be harnessed with the premise of controllable synthesis of SWCNTs, where catalyst composition thermodynamically plays a vital role. Herein, we have systematically investigated the effects of catalyst composition on SWCNTs synthesis, using a novel floating-catalyst chemical vapor deposition (FCCVD) system, consisting of catalyst synthesis via spark generator, FCCVD reactor and a real-time monitor of catalysts and SWCNTs. We synthesized SWCNTs from both monometallic (Fe, Co, Ni), bimetallic (Co-Ni, Co-Fe) catalyst particles and kinetically optimized yield and performance of SWCNTs films. We found that the highest yield of SWCNTs from Fe is 15 times as that of Ni SWCNTs and the Co-Ni SWCNTs film possesses best opto-electronic performance. Interestingly, the mean diameter of SWCNTs was found related to the catalyst particle size distributions, but not composition. Moreover, detailed atomic structures determination revealed that SWCNTs from Fe and Co have a wide chirality distribution spanning from zig-zag to armchair edges. However, Co-Ni SWCNTs have comparatively narrower chirality distribution having 71% SWCNTs in the chiral angle of 15-30°. Our results indicate that catalyst composition can efficiently tune yield and characteristics of SWCNTs, but it does not dramatically shift chirality of FCCVD SWCNTs.

1. Introduction

Since their discovery by Sumio Iijima in 1993 [1], single-walled carbon nanotubes (SWCNTs) have attracted a great deal of attention owing to their excellent mechanical,

---

* Corresponding author.
E-mail addresses: esko.kauppinen@aalto.fi (Esko I. Kauppinen), qiang.zhang@aalto.fi (Qiang Zhang)

electrical, thermal and optical properties [2]. The properties of SWCNTs are mainly dependent on their morphology and chirality. Therefore, in last few decades significant efforts have been devoted to control their morphology and chirality during synthesis [3–5]. In this regard, the most important parameters which have been mainly focused are the size, composition and structure of catalyst particles [5–8], selection of carbon feedstock [9,10] and the synthesis technique.

Chemical vapor deposition (CVD) technique is one of the most commonly used processes for the synthesis of SWCNTs. Based on the catalyst location, CVD is further divided into supported [3–5,7] and floating-catalyst (FCCVD) [9–11] methods. In supported-CVD, the catalysts are prepared and reduced before SWCNT synthesis, which makes this multi-step method tedious. Moreover, interactions between catalyst particles and support makes the synthesis process more complicated [12]. On the other side, FCCVD is a single-step, scalable method in which the entire process of catalyst and SWCNTs formation takes place in a gaseous environment [9,13]. In addition, FCCVD promises yielding highly pure products without contaminations.

It has been observed that the proper choice of catalyst particles plays a significant role in controlling the morphology and chirality of SWCNTs [11,13–15]. Specifically, bimetallic catalysts have shown more promising results to grow narrow chirality of SWCNTs [11]. Normally, catalyst particles in FCCVD are obtained by decomposition of volatile organometallic compounds such as ferrocene and nickelocene etc. [11,13]. However, with this conventional method of nanoparticle fabrication, it is hard to take a full control of composition, number concentration, size and structure of both monometallic and bimetallic nanoparticles. Furthermore, the integrant of catalyst particles is limited because of their toxic precursors. Therefore, only a few papers have presented [11,14,15] results on the effect of metallic and bimetallic catalysts particles on FCCVD grown SWCNTs. However, they produced very low purity of the final product containing a mixture of carbon black powder along with single and multi-walled CNTs, thus SWCNT has to be separated from the mixture through a post synthesis liquid-based sonication-centrifugation-annealing process [11,14,15]. This type of post synthesis separation treatments are not only time-consuming but can also contaminate and damage the nanotubes [16,17]. Also, no detailed atomic structures of the grown SWCNTs were presented as only optical methods were used to characterize the nanotubes [11,14,15].

To overcome the above-mentioned difficulties, we decoupled catalyst particle generation process from SWCNT growth. The catalyst generation was devised by a purpose-built, ex-situ spark discharge generator (SDG), permitting a precise control of catalyst, and thus, SWCNT number concentration during growth [9,18]. In SDG, catalyst particles are produced from physical evaporation-nucleation-condensation of the electrode's material in the presence of some inert or non-reacting carrier gas. Depending on the electrode materials and by tuning other spark parameters (e.g. applied voltage, current, frequency, etc.), we can control composition, size and number concentration of catalyst particles [18]. Moreover, we can measure the size and number concentration of catalyst particles in gas phase by using differential mobility analyzer (DMA) before feeding in the CVD reactor. Therefore, it is a reliable technique to study the effect of catalyst composition, size and concentration on SWCNTs synthesis. So far we synthesized SWCNTs from spark-produced Fe catalyst nanoparticles only with CO as carbon source [9]. The two major problems of using CO as carbon source are its low conversion rate and high toxicity.

In this study, for the first-time we have systematically investigated catalyst composition effects on yield, morphology, helicity and conductivity of single-step grown SWCNTs in FCCVD. For this purpose, we utilized various spark-produced monometallic (iron, cobalt, nickel) and bimetallic (cobalt-nickel, cobalt-iron) catalysts particles [18]. Nitrogen was used as the main carrier gas with 15% of hydrogen and only 0.06% ethylene. Ethylene was employed as a carbon source due to its similarity with CNTs in nature of chemical bonding (i.e. sp^2). Compared to carbon monoxide, ethylene as the carbon source makes the synthesis process more economical and environment friendly. From real-time measurement of the catalyst and SWCNTs number concentration using DMA, we observed that Ni particles have low catalytic activity towards the synthesis of SWCNTs. Whereas, SWCNTs produced from Fe and Co have higher yields and better conductivity of SWCNTs films. Furthermore, for the first-time we utilized Co for SWCNTs synthesis in FCCVD method. Additionally, we made bimetallic nanoparticles of Co with Fe and Ni and we found that Co-Ni bimetallic catalyst particles are more effective to control chiral structure of SWCNTs. Furthermore, we quantitatively compared yield and conductivity of SWCNTs films with various monometallic and bimetallic catalysts particles. Finally, effect of three most auspicious catalysts i.e. Fe, Co and Co-Ni on SWCNTs chirality, morphology and conductivity was studied in detail. More importantly, the atomic structures i.e.

(n, m) indices of the as-synthesized Fe, Co and Co-Ni SWCNTs were determined using a direct method based on electron diffraction technique [19].

2. Experimental section

2.1 Catalyst synthesis

Catalyst particles were prepared in gas phase by the rod-to-tube type spark discharge generator which has been discussed in our earlier work [18]. Rod and tube electrodes (Goodfellow, UK) of highly pure iron (99.8%), nickel (99.5%) and cobalt (99.95%) were used as a source of catalyst particles. Bimetallic Co-Ni and Co-Fe catalysts were synthesized from cobalt rod with Ni or Fe as tube electrode. For material evaporation from electrodes a high voltage source (HV) (Heinzinger PNC 20000-10 ump) was employed to charge 220 pF external capacitor (C) through 1 MΩ ballast resistor (R). Nitrogen (99.995%) was used as carrier gas to produce catalyst particles in spark discharge generator. The regulation of carrier gas (1.5-2 lpm) through the spark chamber was maintained by a mass flow controller (Aalbrog GFC37 (N_2)). The complete set up for particles production is shown schematically in Fig. 1.

2.2 SWCNTs synthesis

SWCNTs were synthesized in a vertical FCCVD reactor with spark-generated Fe, Co, Ni, Co-Fe and Co-Ni particles as catalysts and 0.1-0.4 sccm (200-800 ppm) ethylene (C_2H_4) (99.999%, AGA) as carbon source. The FCCVD reactor consists of a quartz tube (inner diameter 22 mm) vertically placed inside a 90 cm long high temperature furnace. The temperature of the furnace was set at 1050 ^{o}C. The temperature profile shown in Fig. 1 is the centerline N_2 temperature measured by the 1.5 mm thermocouple at the setting furnace temperature of 1050 ^{o}C. The average residence time in the growth zone (800-1050 ^{o}C) is about 10 seconds.

420 sccm N_2 containing catalyst particles from spark chamber and 80 sccm H_2 (99.999%, AGA) were introduced into the CVD reactor. The remaining N_2 from spark chamber was just guided to exhaust. Gas flows into the reactor were carefully controlled with highly precise mass flow controllers (MFCs). In all cases, the total flow inside the CVD reactor was kept constant at 500 sccm. The schematic for gas flows is shown in Fig. 1.

Gas phase SWCNTs grown in the reactor were directly collected at the outlet of the reactor on nitrocellulose membrane filters (Merck Millipore, France, diameter 13 mm) in the form of thin films. For further characterizations, the SWCNTs were also directly collected on to a TEM grid, or deposited on to Si/SiO$_2$ substrate using thermophoresis technique [20]. To increase the SWCNT films conductivity, they were doped with 16 mM solution of AuCl$_3$ (99.99%, Sigma-Aldrich) in acetonitrile (99.999%, Sigma-Aldrich) by drop-casting technique [21]. After doping for three minutes, films were washed with pure acetonitrile and dried before measuring sheet resistances.

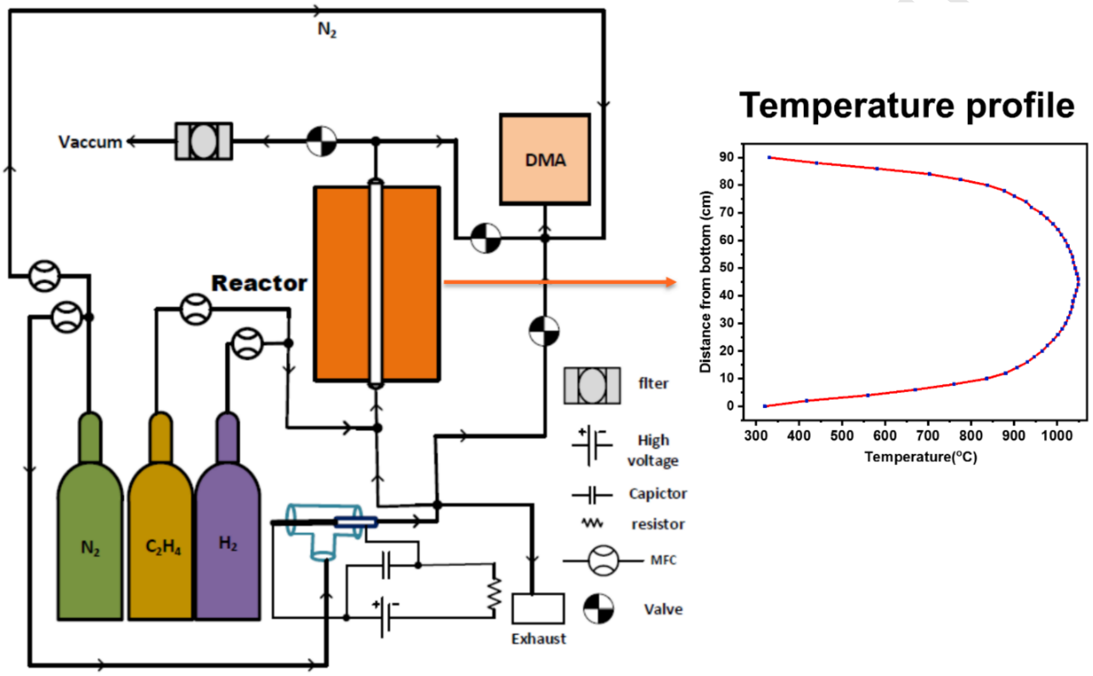

Fig. 1. *Complete set up of spark-FCCVD system for SWCNTs synthesis and temperature profile of the reactor at set temperature of 1050* ^{o}*C. Catalyst particles were produced from purpose-built ex-situ rod-to-tube type spark discharge generator and then introduced in to the vertical FCCVD reactor for the gas phase synthesis of SWCNTs.*

2.3. Characterizations

2.3.1 Real-time measurement of catalyst particles and SWCNTs number size distribution

The catalyst particle number size distribution (NSD) were monitored in real time by scanning mobility particle sizer with Faraday cup electrometer (SMPS+FCE, the GRIMM Aerosol Technic GmbH, Germany). To measure NSD and total number concentration (NC) of the catalyst particles, 1 lpm flow of the aerosol from spark discharge generator was directly introduced into SMPS+FCE. In addition, SMPS+FCE was also employed to characterize SWCNTs total NC and yield in gas phase with similar process.

2.3.2 Optical characterizations

For optical characterizations, SWCNTs thin films collected on membrane filters were directly transferred on transparent quartz slides (HQS300, Heraeus) by dry press-transfer technique [22]. Optical absorption spectra (OAS) and transmittance of the SWCNTs films were measured by Agilent Carry 5000 UV-vis-NIR spectrometer (Agilent Technologies, Inc.). Raman spectra of SWCNTs was obtained by Horiba Labram-HR 800 (Horiba Jobin-Yvon) Raman spectrometer by three different excitation lasers with wavelengths of 488, 514 and 633 nm.

2.3.3 Electron microscopy for morphology and chirality of SWCNTs

The bundle length of SWCNTs were measured by a scanning electron microscope (Zeiss Sigma VP, Carl Zeiss GmbH, Germany). Whereas, for bundle diameters and electron diffraction (ED) of SWCNTs, and for X-rays energy dispersive spectrum (EDS) of the catalyst nanoparticles, double aberration-corrected high-resolution transmission electron microscope (HRTEM) (JEOL-2200FS, JEOL Ltd., Japan) was employed.

2.3.4 Measurement of sheet resistances

Sheet resistances of the SWCNTs transparent conductive films (TCFs) were measured by 4-point probe (Jandel Engineering Ltd, UK, tip radius 250 µm, tip spacing 1 mm) connected to a multi-meter (HP/Hewlett Packard 3485A). A set of data points were obtained by analyzing SWCNTs films with various thickness and transmittance. Data points were nonlinearly fitted using the method described in the literature [22].

3. Results and discussions

3.1 Optimization of the synthesis parameters

Here, the synthesis process is optimized based on the film performance, i.e. to minimize the sheet resistances of SWCNT films with 90% transmittance (@ 550 nm wavelength). For quantitative research and comparison, all catalyst particles were preset to the same size (distributions) and concentration, as shown in Fig. 2a. For minimum sheet resistances, the required flow rate of H_2 is 80 sccm and for N_2 is 420 sccm at a setting furnace temperature of 1050 ^{o}C. The optimized amount of C_2H_4 for monometallic catalysts: Fe and Co is 0.1 sccm (200 ppm), for Ni is 0.4 sccm (800 ppm), whereas, for bimetallic catalysts: Co-Ni and Co-Fe is 0.3 sccm (600 ppm). The results and discussion below are based on the optimized synthesis conditions.

3.2 SWCNT yield and performance

SWCNTs yield were compared among various catalysts and the result is Fe>Co-Fe> Co>Co-Ni>Ni, as shown in Fig. 2b and S1. For all catalysts, the geometric mean mobility diameter (D_{ME}) of particles was adjusted to 3.5 nm with a total NC of ~4.3×10^{6} cm^{-3} before feeding into the FCCVD reactor. We found that as-synthesized SWCNTs from Fe, Co, Co-Fe and Co-Ni catalysts have similar D_{ME} of $\sim 45\ nm$. Also, NC of SWCNTs from Fe, Co, Co-Fe are comparable, but NC of Co-Ni CNT is slightly lower. However, SWCNTs synthesized from Ni were found utterly different. Ni SWCNTs have very small D_{ME} ($\sim 15\ nm$) and much lower NC compared to SWCNTs from other catalysts. D_{ME} of CNT is correlated to their bundle length (l) by a mathematical relation $D_{ME} \propto \sqrt[3]{l}$ [23]. Hence, DMA result indicates that SWCNTs from Ni have shorter length compared to SWCNTs produced from other catalysts.

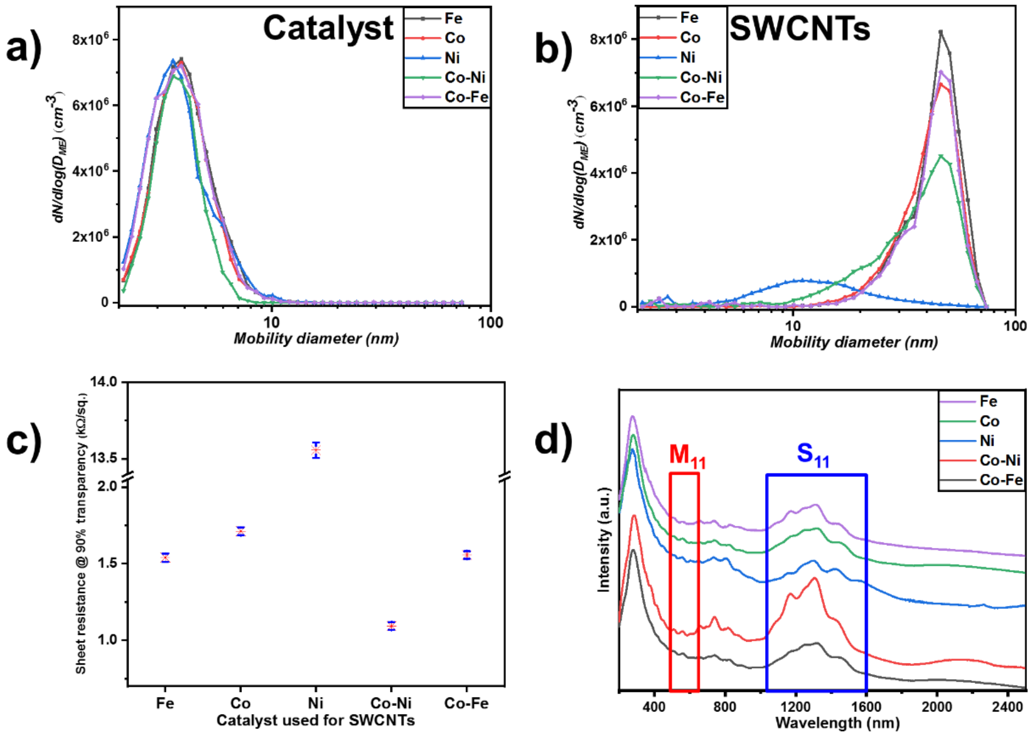

*Fig. 2. A comparison between number size distributions of **a)** catalyst particles (Fe, Co, Ni, Co-Ni & Co-Fe) and **b)** as-produced SWCNTs with various catalysts in gas phase. **c)** Sheet resistance of pristine Fe, Co, Ni, Co-Ni & Co-Fe SWCNT films with 90% transmittance (@ 550 nm wavelength). **d)** Optical absorption spectra of as-grown SWCNTs showing first semiconducting (S_{11}) and metallic (M_{11}) transitions peaks.*

Furthermore, the quantitative comparison of the SWCNTs yield was also carried out by collecting sample on the membrane filter (13 mm diameter) for a fixed time. Depending on NC of SWCNTs from various catalysts, the film thickness and optical transmittance were different. Therefore, based on optical transmittance data, we obtained normalized yield and it has been provided in supporting information as Fig. S1. The data revealed that yield of SWCNTs from Fe is ~15 times higher than that from Ni having poor catalytic activity towards SWCNT synthesis. Since, for the transition metals, carbon solubility decreases from left to right in periodic table [24,25] and Ni has lower carbon solubility than Fe and Co. Therefore, we propose that Ni showed poor catalytic activity towards SWCNT synthesis and as a result, we got comparatively, lower SWCNT yield and shorter bundle length.

Moreover, we compared sheet resistance of the pristine SWCNT films from various catalysts which is plotted in Fig. 2c. We found that the opto-electronic performance of the SWCNT films from Fe, Co, Co-Fe and Co-Ni is superior to that of the Ni SWCNT films, owing to the short length of nanotubes from Ni catalysts. Hence, in our case, Ni SWCNTs are not a good choice for TCFs applications. For the comparison of SWCNTs diameters with various catalysts we obtained their optical absorption spectra (OAS) as shown in Fig. 2d. Since the mean diameter of the nanotubes is strongly correlated with the position of first inter-band transitions in semiconducting (S_{11}) and metallic (M_{11}) nanotubes and we did not observe any prominent shift in S_{11} and M_{11} peaks positions with the change in catalysts. It means that as-grown SWCNTs with various catalysts have similar average diameter and their diameter is around 1 nm, analyzed from Kataura plots [26,27]. The OAS result indicates that, in our case, the diameter of SWCNTs is dominantly controlled by the size of catalyst particles rather than catalyst composition.

Transition metals Fe, Co and Ni as catalysts for SWCNT synthesis are cheap, easily available and highly active which has been proved in supported-CVD process [25,28]. But our results show that spark-produced Ni is not a highly active catalyst for FCCVD growth of SWCNTs. On the other hand, Fe is an extensively studied catalyst in spark [9,18,29] and ferrocene ($Fe(C_5H_5)_2$) [16,30] based FCCVD methods. Our earlier work showed that ferrocene based Fe catalyst particles with ethylene as carbon source are not effective to control chiral structure of SWCNTs [30]. Therefore, to synthesize bimetallic catalyst particles Co was selected as major catalyst which have never been studied in FCCVD method for SWCNT synthesis. We combined Co with Fe and Ni to produce Co-Fe and Co-Ni catalyst particles. The integrant in bimetallic catalyst particles were confirmed by scanning TEM-EDS analysis and plotted as Fig. S2 in supporting information.

Compared to pure Co catalyst, Co based bimetal catalysts give lower SWCNTs yield but better performance of SWCNT films. Specifically, Co-Ni based SWCNT film has much better performance than Co-Fe and Co based ones as shown in Fig. 2c. It's worth mentioning here that for optimized conditions with similar NC and size of five different catalysts (Fe, Co, Ni, Co-Ni and Co-Fe) there are noticeable changes in NC of SWCNTs. It means that catalyst composition can significantly affects C_2H_4 decomposition and nucleation of SWCNTs. More importantly, we observed that Co-Ni SWCNTs gave relatively higher S_{11} peak compared to other SWCNTs in OAS (Fig. 2d), indicating that Co-Ni may produce SWCNTs enriched with some specific chiralities. However, SWCNTs produced by Co-Fe and Co catalyst particles have very similar absorption spectra. Also, Co-Fe CNTs performance lies in between that is pure Co and Fe SWCNTs (Fig. 2c). Based on above mentioned comparative analysis of SWCNTs yield, performance and OAS with five catalysts, three kinds of SWCNTs (i.e. Fe, Co and Co-Ni) were characterized in more detail, to investigate effect of catalyst composition on SWCNTs morphology, chirality and conductivity. The selection was made on the basis of better performance with reasonable yield and having distinctive optical absorption peaks.

3.3 The change in morphology of SWCNTs with the catalysts

We investigated the effect of catalyst composition on bundle length and diameter of carbon nanotubes grown with Fe, Co, and Co-Ni catalysts particles. The bundle length comparison of SWCNTs was made from SEM by measuring length of 200-220 bundles directly collected on to Si/SiO_2 substrate. The results obtained are plotted as a bundle length distribution in Fig. 3b, c and d with Fe, Co and Co-Ni as the catalysts, respectively. A typical SEM image used for the bundle length analysis is also shown in Fig. 3a.

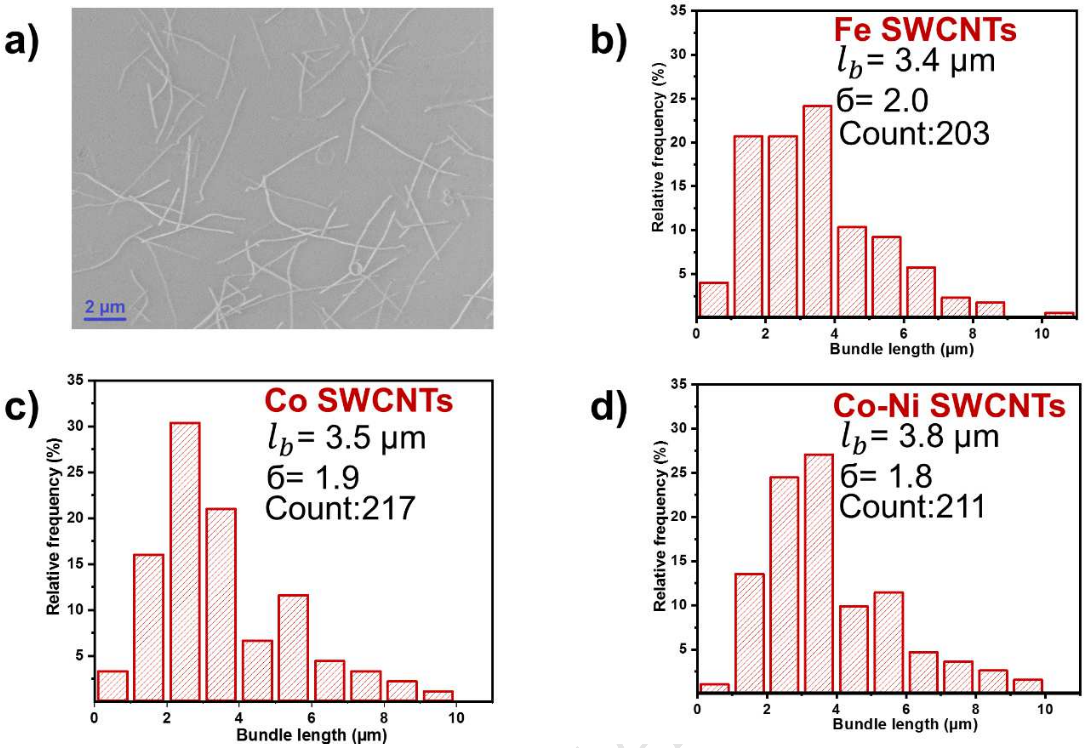

Fig. 3. a) *A SEM image of SWCNTs deposited on to Si/SiO$_2$ substrate. Bundle length distribution and mean bundle length* (l_b) *of SWCNTs produced by* ***b)*** *Fe (3.4 µm),* ***c)*** *Co (3.5 µm) and* ***d)*** *Co-Ni (3.8 µm) as catalysts particles.*

We observed a slight shift in average bundle length (l_b) of the nanotubes by changing catalyst. The nanotubes produced by Fe have shortest l_b of 3.4 µm. Whereas, Co SWCNTs have l_b 3 .5 µm and longest tubes (3.8 µm) were found in case of Co-Ni as catalyst.

For the measurement of mean bundle diameter (d_b) and bundle diameter distribution of the nanotubes, HRTEM was used. In all three cases, d_b was carefully measured by analyzing 170-180 HRTEM micrographs. A typical HRTEM image of a single and a SWCNT bundle is shown in Fig. 4a. The variation in bundle diameter distribution of SWCNTs with Fe, Co and Co-Ni catalysts is plotted in Fig. 4b, c and d, respectively. Diameter distribution revealed that Co SWCNTs have comparatively larger $d_b (4.4\ nm)$ with only 12% individual nanotubes. Whereas, for Fe and Co-Ni SWCNTs d_b is $4.1\ nm$ and $4.0\ nm$ with approximately14% of individual nanotubes.

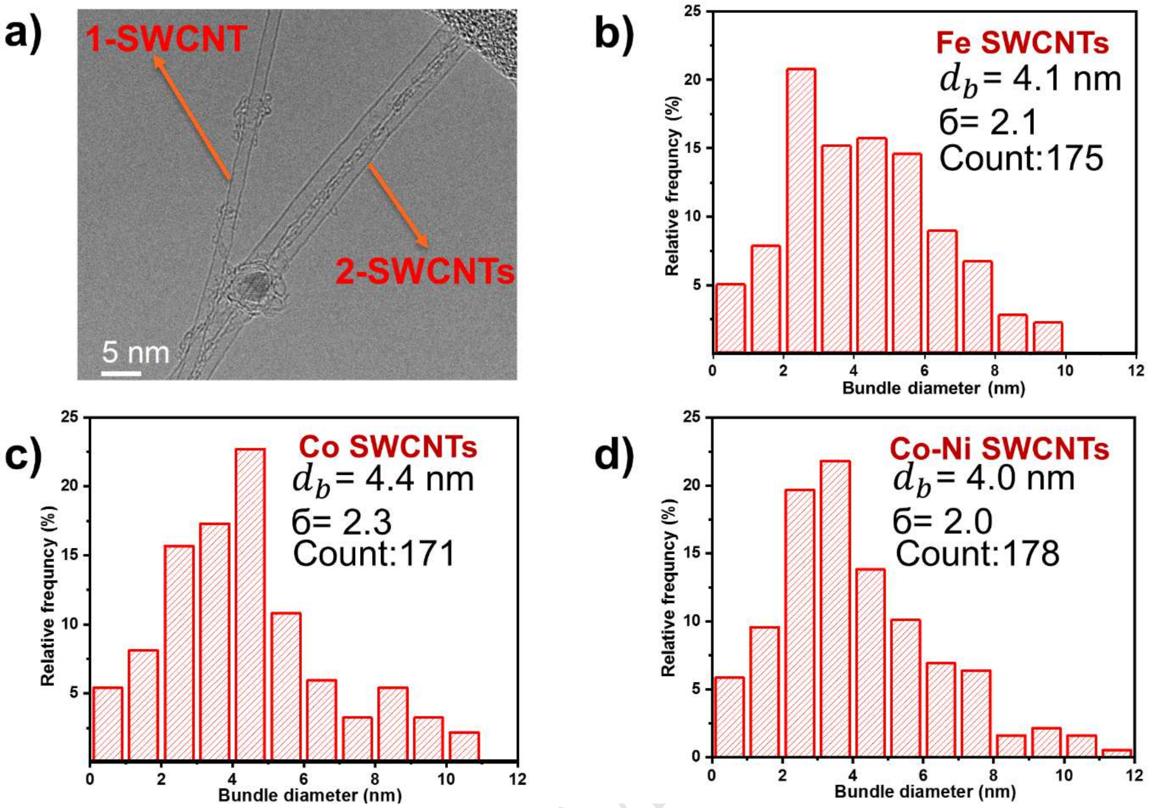

Fig. 4. a) *A typical high-resolution transmission electron microscope (HRTEM) image of a bundled and an individual SWCNT. Bundle diameter distribution and mean bundle diameter* (d_b) *of FCCVD grown SWCNTs with* ***b)*** *Fe (4.1 nm),* ***c)*** *Co (4.4 nm) and* ***d)*** *Co-Ni (4.0 nm) as catalysts.*

Another very important parameter for many applications is the SWCNT diameter which is also investigated here. The variation in diameter of the SWCNTs was compared by using OAS, Raman spectra and analysis of ED data. In OAS the most intense S_{11} peak for both Fe and Co SWCNTs lie at $1322\,nm$, corresponding to $1.01\,nm$ mean diameter. This result is consistent with the result obtained through supported-CVD method where different ratios of Co and Fe did not affect diameter of SWCNTs [31]. But for Co-Ni SWCNTs, maximum intensity peak is at $1305\,nm$, corresponding to $0.98\ nm$ mean diameter. Such small diameter nanotubes (≈ 1 nm) owing to large bandgap are very useful for many potential applications, for instance, in photovoltaic devices [8]. Radial breathing mode (RBM) of Raman spectra with three different lasers $(633, 514\ \&\ 488\,nm)$ was also analyzed to get diameter range of as-synthesized SWCNTs with different catalysts. The diameter (d) of SWCNTs is inversely proportional to

RBM frequency (ω) through the relation $\omega = 217.8/d + 15.7$ [32]. The diameter range by RBM frequency from Fig. 5a, b & c, with all three catalysts is from $0.75\,nm$ to $1.65\,nm$. However, it can be seen that the relative abundance of specific diameter nanotubes varies with the change in catalysts.

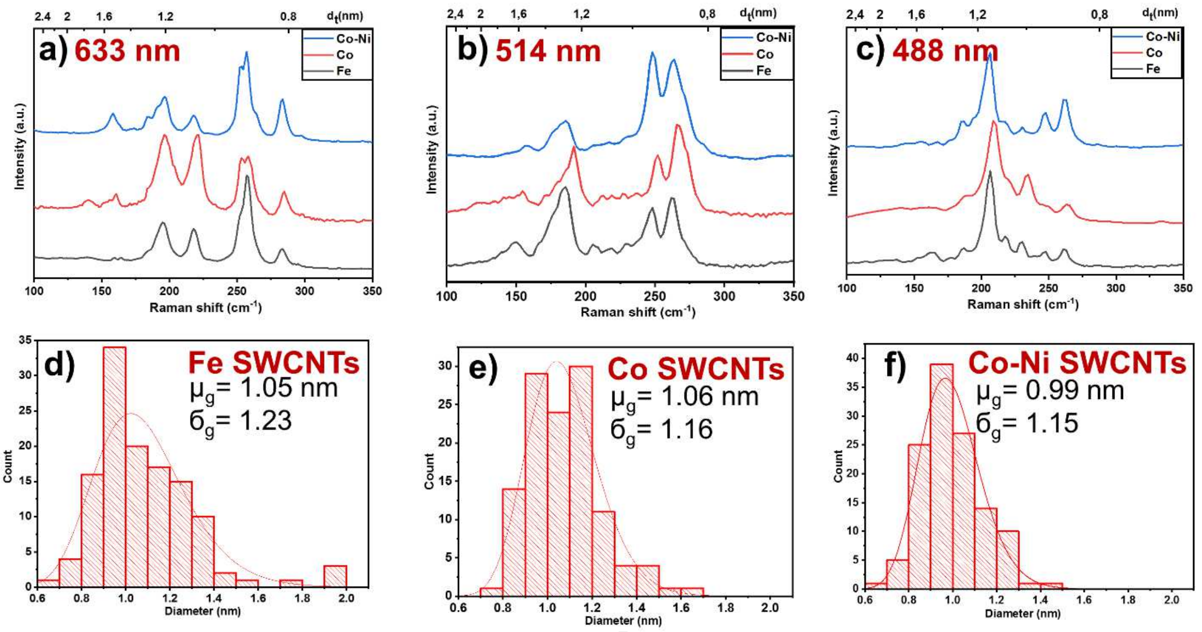

*Fig. 5. Radial breathing mode (RBM) in Raman spectra of as-synthesized various SWCNTs using **a)** 633 **b)** 514 & **c)** 488 nm lasers. Diameter distribution from electron diffraction and geometric mean diameter* (μ_g) *of SWCNTs with **d)** iron (1.05 nm), **e)** cobalt (1.06 nm) and **f)** cobalt-nickel (0.99 nm) as catalyst.*

We also quantified diameter distribution of various types of SWCNTs using ED data which is more advanced, accurate and precise technique [19,33]. For this purpose, 125 Fe, 116 Co, and 123 Co-Ni based randomly selected individual SWCNTs were characterized. The diameter distribution obtained from ED statistics with Fe, Co and Co-Ni SWCNTs is plotted in Fig. 5d, e and f, respectively. Interestingly, we found that there is no remarkable change in geometric mean diameter (μ_g) of SWCNTs with the change in catalyst from Fe ($1.05\,nm$) to Co ($1.06\,nm$). However, the Fe SWCNTs have wider diameter range from $0.67 - 2.0\,nm$ with 45% SWCNTs having $d < 1\,nm$ and geometric standard deviation ($б_g$) of 1.23. Whereas, for the case of Co SWCNTs diameter distribution lies in between 0.78 to 1.65 nm with a $б_g$ of 1.16 having 36% SWCNTs with $d < 1\,nm$. From ED, the Co-Ni SWCNTs have comparatively small

μ_g of 0.99 nm with narrower diameter distribution (σ_g 1.15). The percentage of the SWCNTs having $d < 1\ nm$ increased to 57. The most interesting result obtained from ED is that Co and Co-Ni can produce SWCNTs with much narrower diameter distribution compared to Fe. Such small-diameter FCCVD-SWCNTs having narrow distribution synthesized in this work have never been reported before.

3.4 Tuning chirality of SWCNTs by monometallic and bimetallic catalyst particles

The chirality of FCCVD-grown SWCNTs is also catalyst dependent. The chiral structure of SWCNTs was studied by ED technique through analyzing more than 115 individual, clean, and straight tubes from each sample. The results obtained from the ED analysis are plotted as chirality maps with Fe, Co and Co-Ni in Fig. 6a, b and c along their chiral angle distribution in Fig. 6d, e and f, respectively. Based on an unambiguous intrinsic layer-line spacing analysis method [19], the representative diffraction patterns of the zig-zag, chiral and armchair nanotubes with their (n, m) indices are displayed in the Fig. 6g, h and i. ED analysis revealed that Fe SWCNTs are distributed with 12% nanotubes having (8, 6), (9, 5) and (10,4) chiralities. Most of them are clustered near 1 nm region but few have very small (≈ 0.67 nm) or large (≈ 1.85 nm) diameters as well. The fraction of semiconducting tubes is 61% with the mean chiral angle of 16.06 ± 8.35^{o} having no preference towards the zig-zag or armchair edges. Our result is consistent with the reported result in the literature by Aqeel *et al.* using ethylene as carbon source and ferrocene ($Fe(C_5H_5)_2$) as catalyst precursor [30]. Hence, our result indicates that in FCCVD method selection of catalyst precursor has no role in tuning chirality distribution of SWCNTs.

Co SWCNTs have comparatively narrow chirality distribution. A very high fraction (71%) of SWCNTs lie in 0.3 nm diameter interval starting from 0.9-1.2 nm as shown in Fig. 5e. 15% of the Co nanotubes are enriched with (9, 8), (11, 5) and (9, 7) chiralities. Some chiralities with very small or big diameter, for example (8, 1), (8, 2), (7, 4), (21, 2) and (17, 11) etc. which were found in Fe sample were absent in Co sample. Also, most abundant chiralities in Fe SWCNTs (8, 6), (10, 4) and (9, 5) account for only 6% in Co sample. But similar to Fe SWCNTs, Co SWCNTs are also randomly oriented from zig-zag to armchair having the mean chiral angle 15.78 ± 9.06^{o} with 60% semiconducting tubes.

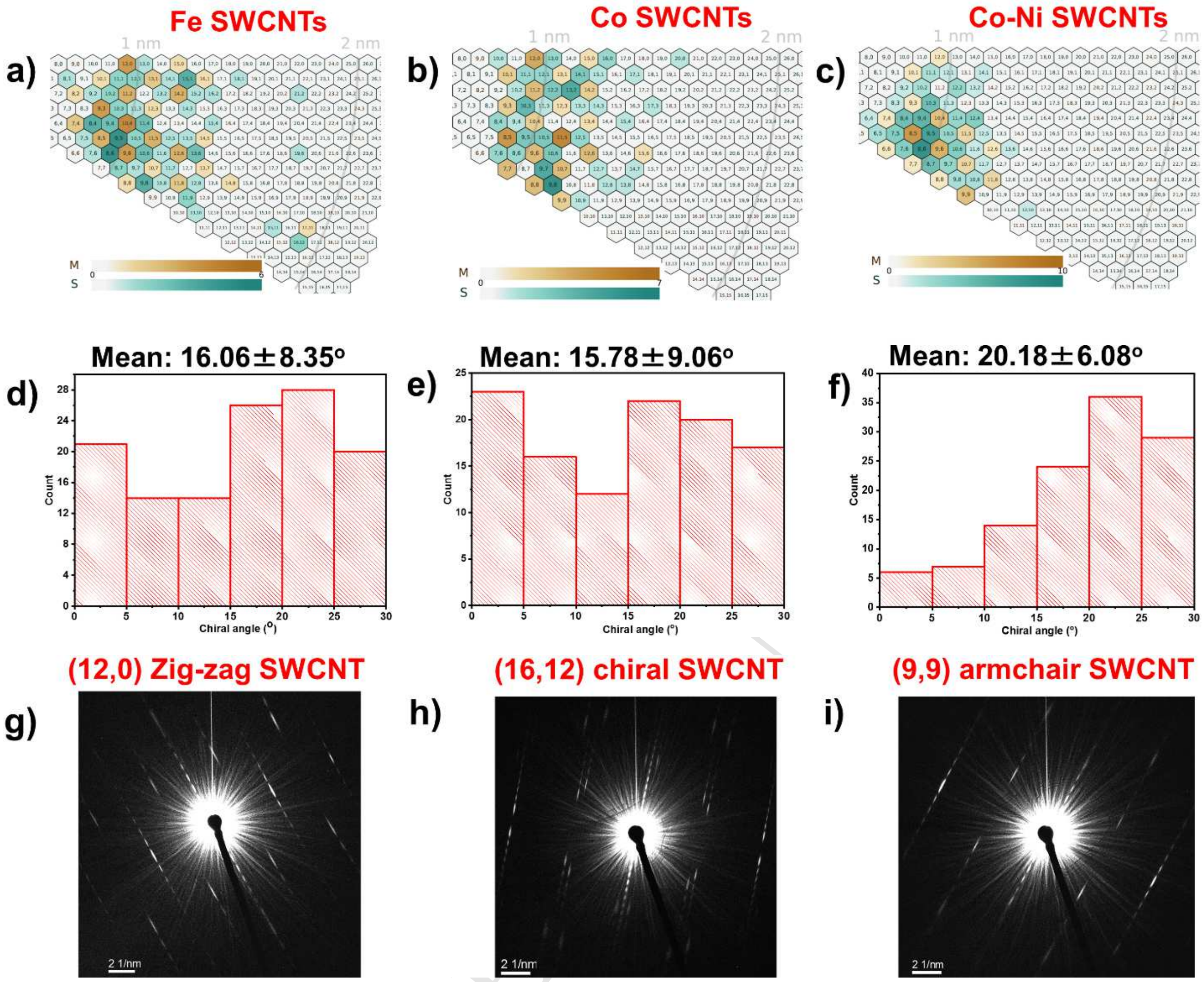

Fig. 6. *Chirality distribution maps and chiral angle distribution of individual SWCNTs based on* ***a)*** *&* ***d)*** *monometallic Fe,* ***b)*** *&* ***e)*** *monometallic Co and* ***c)*** *&* ***f)*** *bimetallic Co-Ni as catalyst particles. Representative diffraction patterns of the selective* ***g)*** *zig-zag (12, 0),* ***h)*** *chiral (16, 12), and* ***i)*** *armchair (9, 9) SWCNTs.*

The most promising results were from Co-Ni bimetallic catalyst particles. We found that Co-Ni can produce SWCNTs with narrower chirality and diameter distributions than Co and Fe. In this case, 73% of SWCNTs have narrow diameter ranging from 0.8-1.1 nm and we found that 71% of the tubes lie in the chiral angle from 15-30^{o} with the mean chiral angle of 20.18±6.08^{o}. Furthermore, fraction of semiconducting nanotubes is 69%. It is interesting to note that out of 123 nanotubes, only a single nanotube has zig-zag structure of (12, 0). The most dominant chiralities from Co-Ni which are 20% of the total tubes are (8, 5), (8, 6) and (9, 5). The possible reason of getting narrow chirality with Co-Ni might be due to synergistic effects of two metals, resulting in activation of small catalyst area as has been proposed in supported-CVD growth process [8,34]. Also, the higher fraction of near-armchair nanotubes is the frequently observed phenomenon in chiral-selective growth of SWCNTs and has been attributed to thermodynamic stability of near arm-chair nanotubes [35]. Moreover, by comparison of chirality maps in Fig. 6b and c, it can be seen that we can increase smaller diameter nanotubes ($< 0.75\,nm$) with the change in catalyst from Co to Co-Ni. Some specific small diameter nanotubes having chiralities (6, 4), (6, 5), and (6, 6) were only found with bimetallic Co-Ni catalyst. The detailed statistics on change in individual chirality with different catalysts is provided in supporting information (Fig. S3-S5).

Hence, we conclude that similar to supported-CVD methods [5–7] chirality is tunable in FCCVD with the change in catalyst composition. But for very high selectivity in FCCVD, further research needs to be carried out, such as more control on catalyst size and structure. Moreover, comparison of chirality distribution of spark based Fe SWCNTs in this work using ethylene and in our earlier work with CO [9] show that carbon source also plays significant role in tuning chirality distribution of SWCNTs. The reason might be very different products obtained as a result of CO and ethylene decomposition at high temperature in the synthesis reactor.

3.5 Catalyst effect on SWCNTs based TCFs

From the above analysis, we observed that the change of catalysts affects yield, bundle length, bundle diameter and chirality of SWCNTs. The conductivity of SWCNTs based films is mainly dependent on their morphology [36] and structure [16]. For better conductivity, SWCNTs with high fraction of individual nanotubes or small bundled, having large tube diameter, and long length are more preferred [37]. To further gain insight on the effect of catalyst on SWCNTs TCFs, we fabricated films with various transparencies by collecting samples on the membrane filter for different collection times. The films from membrane filters were directly transferred on transparent quartz slides by a dry press-transfer technique [22] for measuring % transmittance (T). A plot of data points having different % T versus sheet resistance (R_s) with various types of SWCNTs is shown in Fig.7a. Data points were fitted by the relation $R_s = -1/KlnT$ where, K is constant of proportionality which depends on optical and electrical properties of SWCNTs [22]. A representative SEM image of 97% transparent SWCNTs film is also displayed in Fig. 7b.

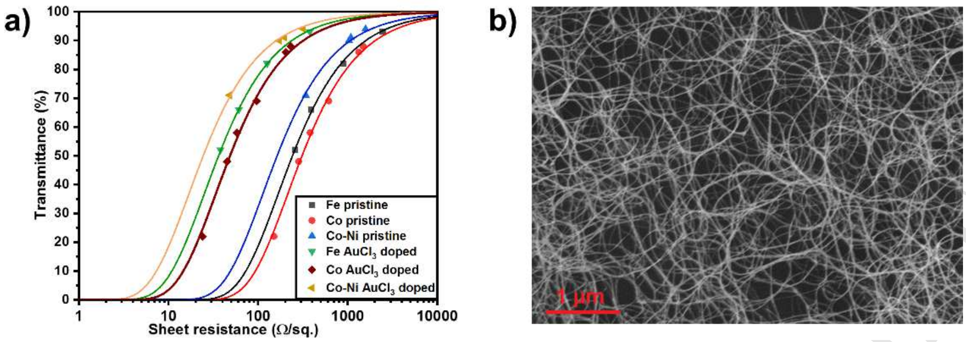

Fig. 7. a) *The sheet resistance (Ω/sq.) vs. transmittance (%) at 550 nm wavelength of pristine and* $AuCl_3$ *doped SWCNTs based transparent conductive films using Fe, Co and Co-Ni as catalyst particles.* ***b)*** *An SEM image of 97% transparent conductive film showing very clean, long and randomly oriented network of SWCNTs.*

As, can be seen from Fig. 7a, the pristine R_S value of the 90% transparent (@ 550 nm) Co-Ni SWCNT film (1090 Ω/sq.) is much lower than Fe (1512 Ω/sq.) and Co ((1704 Ω/sq.) SWCNT films. The Co-Ni SWCNTs films were found to have lowest R_S value because Co-Ni SWCNTs have little defects (Fig. S6), long bundle length (3.8 µm), and small bundle diameter (4.0 nm). To further improve the conductivity, we doped SWCNTs film with $AuCl_3$ which is considered to be a more stable dopant for SWCNTs [21]. Doping of SWCNTs with $AuCl_3$ shifts the Fermi level of both metallic and semiconducting nanotubes down towards valance band [38] which helps in improving conductivity of the film. The doping factor (R_S ratio of pristine and doped films) for our SWCNTs is ~6 and we could not find any observable difference in the doping factor with the change in catalyst. After doping @ 90% transparency, minimum R_S value was found with bimetallic Co-Ni (172 Ω/sq.) and then with monometallic Fe (243 Ω/sq.) and Co (274 Ω/sq).

4. Conclusion

We have, for the first time, successfully synthesized SWCNTs from a variety of spark-produced monometallic (Fe, Co, Ni) and bimetallic (Co-Ni, Co-Fe) catalyst particles using ethylene as carbon source. We systematically studied effects of catalyst composition on yield, morphology, chirality and conductivity of single-step grown-SWCNTs from various catalyst particles. It was observed that spark-produced Ni catalyst particles show poor catalytic activity for SWCNT growth. Interestingly, the mean diameter of SWCNTs is independent of catalyst composition under similar catalyst size distributions. However, the Co-Ni SWCNTs show narrower diameter distribution than the others. In addition, Co-Ni SWCNTs present comparatively small bundle diameters, long bundle length, little defects, resulting in better TCFs performance. Furthermore, unambiguous electron diffraction analysis demonstrated that as-grown SWCNTs from monometallic (Fe and Co) have a wide chirality distribution spanning from zig-zag to armchair. On the contrary, with bimetallic Co-Ni catalyst, we observed that the chirality distribution is slightly skewed favoring large chiral angles with 71% SWCNTs lying in the range from 15-30^o. Moreover, fraction of semiconducting SWCNTs from Co-Ni is 69% compared to 61% with Fe and Co as catalyst. To summarize, in our spark-discharge- based FCCVD, the catalyst composition plays significant roles in tuning SWCNTs yield, quality and opto-electronic performance of the SWCNTs film while SWCNTs morphology is less dependent on the catalyst composition. Moreover, in FCCVD catalyst composition can tune relative abundance of specific chiralities, but it does not dramatically change chirality of SWCNTs, which is significantly different from that in supported-CVD growth process.

Acknowledgements

The research leading to these results has received funding from European Union Seventh Framework Program under Grant Agreement No. 604472 (IRENA project), and the Aalto Energy Efficiency (AEF) Research Program through the MOPPI project. The research has also been partially supported by Academy of Finland via projects 286546 (DEMEC), and 292600 (SUPER) as well as by TEKES Finland via projects 3303/31/2015 (CNT-PV) and 1882/31/2016 (FEDOC). This research also got partial support from HEAL department Khyber Pakhtunkhwa, Pakistan through notifiaction No.SO(Trg)HE/1-10/Ph.D Scholarships/2012. This work made use of the Aalto University Nano-microscopy Center (Aalto-NMC) premises.

References

[1] S. Iijima, T. Ichihashi, Single-shell carbon nanotubes of 1-nm diameter, Nature. 363 (1993) 603–605. doi:10.1038/363603a0.

[2] R. Rao, C.L. Pint, A.E. Islam, R.S. Weatherup, S. Hofmann, E.R. Meshot, F. Wu, C. Zhou, N. Dee, P.B. Amama, J. Carpena-Nuñez, W. Shi, D.L. Plata, E.S. Penev, B.I. Yakobson, P.B. Balbuena, C. Bichara, D.N. Futaba, S. Noda, H. Shin, K.S. Kim, B.

Simard, F. Mirri, M. Pasquali, F. Fornasiero, E.I. Kauppinen, M. Arnold, B.A. Cola, P. Nikolaev, S. Arepalli, H.-M. Cheng, D.N. Zakharov, E.A. Stach, J. Zhang, F. Wei, M. Terrones, D.B. Geohegan, B. Maruyama, S. Maruyama, Y. Li, W.W. Adams, A.J. Hart, Carbon Nanotubes and Related Nanomaterials: Critical Advances and Challenges for Synthesis toward Mainstream Commercial Applications, ACS Nano. (2018) acsnano.8b06511. doi:10.1021/acsnano.8b06511.

[3] F. Yang, X. Wang, J. Si, X. Zhao, K. Qi, C. Jin, Z. Zhang, M. Li, D. Zhang, J. Yang, Z. Zhang, Z. Xu, L.M. Peng, X. Bai, Y. Li, Water-Assisted Preparation of High-Purity Semiconducting (14,4) Carbon Nanotubes, ACS Nano. 11 (2017) 186–193. doi:10.1021/acsnano.6b06890.

[4] K. Hata, D.N. Futaba, K. Mizuno, T. Namai, M. Yumura, S. Iijima, Water-assisted highly efficient synthesis of impurity-free single-walled carbon nanotubes, Science (80-.). 306 (2004) 1362–1364. doi:10.1126/science.1104962.

[5] F. Yang, X. Wang, D. Zhang, J. Yang, D. Luo, Z. Xu, J. Wei, J.Q. Wang, Z. Xu, F. Peng, X. Li, R. Li, Y. Li, M. Li, X. Bai, F. Ding, Y. Li, Chirality-specific growth of single-walled carbon nanotubes on solid alloy catalysts, Nature. 510 (2014) 522–524. doi:10.1038/nature13434.

[6] X. Zhao, Y. Liu, R. Cui, Y. Li, Nucleation of copper nanoparticles on quartz as catalysts to grow single-walled carbon nanotube arrays, Carbon N. Y. 110 (2016) 390–395. doi:10.1016/j.carbon.2016.09.036.

[7] M. He, A.I. Chernov, E.D. Obraztsova, J. Sainio, E. Rikkinen, H. Jiang, Z. Zhu, A. Kaskela, A.G. Nasibulin, E.I. Kauppinen, M. Niemelä, O. Krause, Low Temperature Growth of SWNTs on a Nickel Catalyst by Thermal Chemical Vapor Deposition, Nano Res. 4 (2011) 334–342. doi:10.1007/s12274-010-0088-3.

[8] K. Cui, A. Kumamoto, R. Xiang, H. An, B. Wang, T. Inoue, S. Chiashi, Y. Ikuhara, S. Maruyama, Synthesis of subnanometer-diameter vertically aligned single-walled carbon nanotubes with copper-anchored cobalt catalysts, Nanoscale. 8 (2016) 1608–1617. doi:10.1039/C5NR06007A.

[9] K. Mustonen, P. Laiho, A. Kaskela, Z. Zhu, O. Reynaud, N. Houbenov, Y. Tian, T. Susi, H. Jiang, A.G. Nasibulin, E.I. Kauppinen, Gas phase synthesis of non-bundled, small diameter single-walled carbon nanotubes with near-armchair chiralities, Appl. Phys. Lett. 107 (2015). doi:10.1063/1.4926415.

[10] E.X. Ding, H. Jiang, Q. Zhang, Y. Tian, P. Laiho, A. Hussain, Y. Liao, N. Wei, E.I. Kauppinen, Highly conductive and transparent single-walled carbon nanotube thin films from ethanol by floating catalyst chemical vapor deposition, Nanoscale. 9 (2017) 17601–17609. doi:10.1039/c7nr05554d.

[11] W.H. Chiang, R.M. Sankaran, Linking catalyst composition to chirality distributions of as-grown single-walled carbon nanotubes by tuning Ni x Fe 1x nanoparticles, Nat. Mater. 8 (2009) 882–886. doi:10.1038/nmat2531.

[12] W. Zhou, L. Ding, J. Liu, Role of catalysts in the surface synthesis of single-walled carbon nanotubes, Nano Res. 2 (2009) 593–598. doi:10.1007/s12274-009-9068-x.

[13] A.G. Nasibulin, A. Moisala, D.P. Brown, H. Jiang, E.I. Kauppinen, A novel aerosol method for single walled carbon nanotube synthesis, Chem. Phys. Lett. 402 (2005) 227–232. doi:10.1016/j.cplett.2004.12.040.

[14] W.-H. Chiang, M. Sakr, X.P.A. Gao, R.M. Sankaran, Nanoengineering NixFe1-x Catalysts for Gas-Phase, Selective Synthesis of Semiconducting Single-Walled Carbon Nanotubes, ACS Nano. 3 (2009) 4023–4032. doi:10.1021/nn901222t.

[15] W.H. Chiang, R.M. Sankaran, Microplasma synthesis of metal nanoparticles for gas-phase studies of catalyzed carbon nanotube growth, Appl. Phys. Lett. (2007). doi:10.1063/1.2786835.

[16] Y. Liao, H. Jiang, N. Wei, P. Laiho, Q. Zhang, S.A. Khan, E.I. Kauppinen, Direct Synthesis of Colorful Single-Walled Carbon Nanotube Thin Films, J. Am. Chem. Soc. (2018). doi:10.1021/jacs.8b05151.

[17] Q. Zhang, N. Wei, P. Laiho, E.I. Kauppinen, Recent Developments in Single-Walled Carbon Nanotube Thin Films Fabricated by Dry Floating Catalyst Chemical Vapor Deposition, Top. Curr. Chem. (2017). doi:10.1007/s41061-017-0178-8.

[18] S. Ahmad, P. Laiho, Q. Zhang, H. Jiang, A. Hussain, Y. Liao, E.X. Ding, N. Wei, E.I. Kauppinen, Gas phase synthesis of metallic and bimetallic catalyst nanoparticles by rod-to-tube type spark discharge generator, J. Aerosol Sci. 123 (2018) 208–218. doi:10.1016/j.jaerosci.2018.05.011.

[19] H. Jiang, A.G. Nasibulin, D.P. Brown, E.I. Kauppinen, Unambiguous atomic structural determination of single-walled carbon nanotubes by electron diffraction, Carbon N. Y. (2007). doi:10.1016/j.carbon.2006.07.025.

[20] P. Laiho, K. Mustonen, Y. Ohno, S. Maruyama, E.I. Kauppinen, Dry and Direct Deposition of Aerosol-Synthesized Single-Walled Carbon Nanotubes by Thermophoresis, ACS Appl. Mater. Interfaces. 9 (2017) 20738–20747. doi:10.1021/acsami.7b03151.

[21] K.K. Kim, S.M. Yoon, H.K. Park, H.J. Shin, S.M. Kim, J.J. Bae, Y. Cui, J.M. Kim, J.Y. Choi, Y.H. Lee, Doping strategy of carbon nanotubes with redox chemistry, New J. Chem. (2010). doi:10.1039/c0nj00138d.

[22] A. Kaskela, A.G. Nasibulin, M.Y. Timmermans, B. Aitchison, A. Papadimitratos, Y. Tian, Z. Zhu, H. Jiang, D.P. Brown, A. Zakhidov, E.I. Kauppinen, Aerosol-synthesized SWCNT networks with tunable conductivity and transparency by a dry transfer technique, Nano Lett. (2010). doi:10.1021/nl101680s.

[23] A. Moisala, A.G. Nasibulin, S.D. Shandakov, H. Jiang, E.I. Kauppinen, On-line detection of single-walled carbon nanotube formation during aerosol synthesis methods, Carbon N. Y. (2005). doi:10.1016/j.carbon.2005.03.012.

[24] O. V. Yazyev, A. Pasquarello, Effect of metal elements in catalytic growth of carbon nanotubes, Phys. Rev. Lett. (2008). doi:10.1103/PhysRevLett.100.156102.

[25] V. Jourdain, C. Bichara, Current understanding of the growth of carbon nanotubes in catalytic chemical vapour deposition, Carbon N. Y. (2013). doi:10.1016/j.carbon.2013.02.046.

[26] Y. Tian, H. Jiang, J. V. Pfaler, Z. Zhu, A.G. Nasibulin, T. Nikitin, B. Aitchison, L. Khriachtchev, D.P. Brown, E.I. Kauppinen, Analysis of the size distribution of single-walled carbon nanotubes using optical absorption spectroscopy, J. Phys. Chem. Lett.

(2010). doi:10.1021/jz100161p.

[27] H. Kuzmany, W. Plank, M. Hulman, C. Kramberger, A. Gr, P HYSICAL J OURNAL B Determination of SWCNT diameters from the Raman response, Eur. Phys. J. B. 320 (2001) 307–320.

[28] M.G. Rostedt, M.J. Hall, L. Shi, R.D. Matthews, Spark Breakdown Voltage and Surface Degradation of Multiwalled Carbon Nanotube Electrode Surfaces, Int. J. Mech. Aerospace, Ind. Mechatron. Manuf. Eng. 7 (2013) 334–339.

[29] Y. Tian, N. Wei, P. Laiho, S. Ahmad, Y. Magnin, Y. Liao, C. Bichara, H. Jiang, E.I. Kauppinen, Cutting floating single-walled carbon nanotubes with a 'CO2 blade,' Carbon N. Y. 143 (2019) 481–486. doi:10.1016/j.carbon.2018.11.035.

[30] A. Hussain, Y. Liao, Q. Zhang, E.X. Ding, P. Laiho, S. Ahmad, N. Wei, Y. Tian, H. Jiang, E.I. Kauppinen, Floating catalyst CVD synthesis of single walled carbon nanotubes from ethylene for high performance transparent electrodes, Nanoscale. (2018). doi:10.1039/c8nr00716k.

[31] I. Ibrahim, J. Kalbacova, V. Engemaier, J. Pang, R.D. Rodriguez, D. Grimm, T. Gemming, D.R.T. Zahn, O.G. Schmidt, J. Eckert, M.H. Rümmeli, Confirming the Dual Role of Etchants during the Enrichment of Semiconducting Single Wall Carbon Nanotubes by Chemical Vapor Deposition, Chem. Mater. 27 (2015) 5964–5973. doi:10.1021/acs.chemmater.5b02037.

[32] M.S. Dresselhaus, G. Dresselhaus, A. Jorio, A.G. Souza Filho, R. Saito, Raman spectroscopy on isolated single wall carbon nanotubes, Carbon N. Y. (2002). doi:10.1016/S0008-6223(02)00066-0.

[33] Y. Tian, H. Jiang, P. Laiho, E.I. Kauppinen, Validity of Measuring Metallic and Semiconducting Single-Walled Carbon Nanotube Fractions by Quantitative Raman Spectroscopy, Anal. Chem. (2018). doi:10.1021/acs.analchem.7b03712.

[34] M. He, A.I. Chernov, E.D. Obraztsova, H. Jiang, E.I. Kauppinen, J. Lehtonen, Synergistic effects in FeCu bimetallic catalyst for low temperature growth of single-walled carbon nanotubes, Carbon N. Y. (2013). doi:10.1016/j.carbon.2012.10.029.

[35] V.I. Artyukhov, E.S. Penev, B.I. Yakobson, Why nanotubes grow chiral, Nat. Commun. (2014). doi:10.1038/ncomms5892.

[36] Y. Liao, A. Hussain, P. Laiho, Q. Zhang, Y. Tian, N. Wei, E.-X. Ding, S.A. Khan, N.N. Nguyen, S. Ahmad, E.I. Kauppinen, Tuning Geometry of SWCNTs by CO_2 in Floating Catalyst CVD for High-Performance Transparent Conductive Films, Adv. Mater. Interfaces. 1801209 (2018) 1801209. doi:10.1002/admi.201801209.

[37] K. Mustonen, P. Laiho, A. Kaskela, T. Susi, A.G. Nasibulin, E.I. Kauppinen, Uncovering the ultimate performance of single-walled carbon nanotube films as transparent conductors, Appl. Phys. Lett. (2015). doi:10.1063/1.4932942.

[38] K.K. Ki, J.B. Jung, K.P. Hyeon, M.K. Soo, H.Z. Geng, A.P. Kyung, H.J. Shin, S.M. Yoon, A. Benayad, J.Y. Choi, H.L. Young, Fermi level engineering of single-walled carbon nanotubes by AuCl3doping, J. Am. Chem. Soc. (2008). doi:10.1021/ja8038689.